Accepted Manuscript

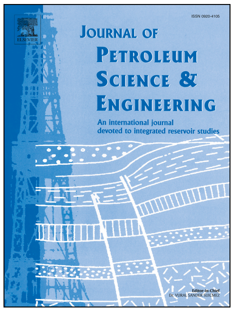

Ultrasonic wave attenuation dependence on saturation in tight oil siltstones

Jing Ba, Rupeng Ma, José M. Carcione, Stefano Picotti

PII: S0920-4105(19)30436-X

DOI: https://doi.org/10.1016/j.petrol.2019.04.099

Reference: PETROL 6038

To appear in: *Journal of Petroleum Science and Engineering*

Received Date: 13 November 2018

Revised Date: 27 March 2019

Accepted Date: 29 April 2019

Please cite this article as: Ba, J., Ma, R., Carcione, José.M., Picotti, S., Ultrasonic wave attenuation dependence on saturation in tight oil siltstones, *Journal of Petroleum Science and Engineering* (2019), doi: https://doi.org/10.1016/j.petrol.2019.04.099.

Ultrasonic wave attenuation dependence on saturation in tight oil siltstones

Jing Ba[a*], Rupeng Ma[a], José M. Carcione[a, b], Stefano Picotti[b]

a. School of Earth Sciences and Engineering, Hohai University, Nanjing, 211100, China.

b. Istituto Nazionale di Oceanografia e di Geofisica Sperimentale (OGS), Borgo Grotta Gigante 42c, Sgonico, Trieste 34010, Italy

Abstract

Ultrasonic P-wave attenuation was measured in tight oil siltstones, carbonates and a tight sandstone with two independent estimation methods. The dependence on saturation in gas-water partially-saturated siltstones at in-situ conditions shows a different behavior compared to the other rocks. The siltstones in our experiments exhibit a behavior characterized by a gradual decrease of attenuation with increasing water saturation in the presence of gas, and full-gas saturation shows more attenuation than full-oil and full-water saturations. However, previous theoretical and experimental studies show that gas-water saturated carbonates and sandstones have the highest attenuation at high water saturations, and generally, a liquid-saturated rock shows more attenuation than a gas-saturated one. Poroelasticity theory shows that the two dominant loss mechanisms (due to fabric heterogeneity and patchy saturation) have peaks at different frequencies for siltstones, resulting in a gradual decrease of attenuation with water saturation, while these mechanisms overlap at ultrasonic frequencies for carbonates and sandstones, leading to an attenuation peak at high water saturations. The predicted attenuation dependence on fluid type agrees with the measurement for most samples. Regarding the tight oil siltstones, although the model fails to explain the experimental results for oil-water saturation, it can be concluded that for gas-water saturation the squirt flow caused by fabric heterogeneity dominates the attenuation, which differs from carbonates and sandstones. Experimental studies show that the attenuation dependence on saturation in tight oil reservoirs can be associated with fabric texture. The theory describes these behaviors, which can potentially improve the practices of detecting and monitoring multi-phase fluids in the reservoirs.

Key words: Elasticity and anelasticity; Microstructure; Permeability and porosity; Acoustic properties; Seismic attenuation; Wave propagation.

*Corresponding author: jba@hhu.edu.cn; jingba@188.com

Introduction

Studies on the effects of minerals, fabric and pore fluid on acoustic wave attenuation in rocks play an important role in fundamental and applied geophysics, since they provide the basic constraints on supporting the quantitative interpretation of subsurface rock properties. For each rock lithology or texture, the attenuation dependence on fluid properties and saturation remains unclear so far.

A number of works (e.g., Nur and Wang, 2001; King, 2005) dealt with the acoustic wave attenuation characteristics in sandstones and carbonates (although wave velocity was always the main issue), with sandstones the most investigated since the 1970s (White, 1975; Winkler and Nur, 1979; Johnston and Toksöz, 1980; Dvorkin and Nur, 1996; Best and Sams, 1997; Tao *et al.*, 1995; Chapman *et al.*, 2016). Carbonates have attracted increasing attention during the last two decades (Cadoret *et al.*, 1998; Agersborg *et al.*, 2008; Adam *et al.*, 2009; Borgomano *et al.*, 2017). On the other hand, there are only few works on tight oil siltstones, which are mainly composed of fine grains of quartz, feldspar and clay. Siltstones have a higher porosity than mud/shale, but have a much lower permeability than sandstone of the same porosity. As an unconventional petroleum resource, there is no consistent strict definition of tight oil. Generally speaking, tight oil refers to the accumulation of oil in a tight rock, whose permeability can be less than 0.1 mD. Reservoir lithology mainly includes tight sandstones, tight siltstones and carbonate rocks with mud. Compared with conventional reservoir rocks, the pore throat diameter is smaller, pore permeability is lower, and mud content is higher (Jia *et al.*, 2012; Zou *et al.*, 2013; Wu *et al.*,2018).

This type of rocks have a great potential as a hydrocarbon source rock, which is of interest to exploration geophysics and geological studies (Clarkson *et al.*, 2012; Cao *et al.*, 2017). To our knowledge, the attenuation dependence on fluid saturation in tight oil siltstones has never been investigated.

Experimental studies on water and gas partially-saturated sandstones and carbonates have shown that compressional (or extensional) wave attenuation generally increases with water saturation and has a peak at high water saturations (Murphy, 1982; Yin *et al.*, 1992; Cadoret *et al.*, 1998; Amalokwu *et al.*, 2014). In most measurements, the attenuation at full liquid saturation is higher than that at full gas saturation (Toksöz *et al.*, 1979; Winkler and Nur, 1982; Adam *et al.*, 2009; Kuteynikova *et al.*, 2014). Different theoretical approaches involving patchy saturation of water and gas (e.g., Norris, 1993; Helle *et al.*, 2003; Müller and Gurevich, 2004; Sun *et al.*, 2014) suggest a similar relationship. However, our measurements on siltstones at in-situ conditions show dependencies distinct from those in coarse-grained rocks (e.g., P-wave attenuation decreases with increasing water saturation), reflecting a different state of wave relaxation.

Siltstones with fine grains and clay have low permeability and are heterogeneous at a submicroscopic scale, leading to different relaxation frequencies compared to sandstones and carbonates. Two distinct squirt-flow mechanisms (crack- and clay-type) were considered by Best (1997) to distinguish clean sandstones/limestones from siltstones with amounts of compliant minerals. The former is the main loss mechanism in sandstones, while the clay-type squirt flow dominates in siltstones.

Furthermore, the low permeability in silt/mud-rocks hinders the migration of light gas in geologic times, and the occurrence of mesoscopic patches, so as to cause grain-size gas pockets at the pore scale, as was recently discussed by Glubokovskikh and Gurevich (2017).

In this work, we estimate P-wave attenuation in partially-saturated siltstones, sandstones and carbonates, at the ultrasonic frequency band (around 1 MHz). The attenuation dependency on saturation in siltstones is compared with that of the coarse-grained carbonates/sandstones, and with published experimental and theoretical studies. The results are interpreted with the poroelasticity theory by incorporating fabric and fluid heterogeneities simultaneously.

Experimental results

Rock samples and experiment procedure

During the last five years, we have performed systematic ultrasonic P- and S-wave measurements on three sets of rock samples, which are listed in Table 1 as set 1 labelled A-L (Ba *et al.*, 2016) (siltstones), set 2 labelled DT1-5 and DS1-3 (Ba *et al.*, 2017) (DT and DS refer to two different types of dolomites), and set 3 labelled DS 4-8 and TSM2 (a tight sandstone), including twelve siltstone samples (25.2 mm in diameter, 50-56 mm long cylinders; collected from tight-oil reservoirs of the Qingshankou Formation, Northeast China), thirteen carbonates (25.2 mm in diameter, 30-42 mm long cylinders; collected from reservoirs of the Ordovician and Cambrian Formations, West China), and one sandstone (25.2 mm in diameter, 42.4 mm long cylinder; collected from a gas reservoir in South China Sea). The samples of set 1 are tested at in-situ conditions, i.e., a confining pressure of 50 MPa, a pore pressure of 25 MPa and a temperature of 80℃. For sets 2 and 3, the experiments are performed at a confining pressure of 80 MPa, a pore pressure of 10 MPa and 20℃ (in-situ confining pressure, pore pressure and temperature are 80 MPa, 40 MPa and 140℃, respectively; a pore pressure of 10 MPa and 20℃ are set in the experiments for safety reasons).

The siltstone samples, composed of fine grains (quartz/feldspar) and clay, have low porosity and very low permeability. The scale of the fabric heterogeneity (i.e. intrapore clay in host rock) is smaller than the pore size (Fig. 1a). In the carbonates (with dissolved pores) and tight sandstone, grain contacts (or microcracks) can be observed (Fig. 1b and 1c). The carbonates and sandstone have coarser grains and higher permeability than the siltstones (see Table 1).

The experimental set-up of Guo *et al.* (2009) is used for the ultrasonic-wave measurements. The procedure of Ba *et al.* (2016) is adopted to measure the ultrasonic waveforms at partial-saturation conditions for samples H-L, DT1-5 and DS1-8 (gas-water and oil-water tests), and TSM2 (gas-water tests). Nitrogen (gas) and kerosene (oil) are used for all the measurements. In the experiments with gas and water saturation, the full water-saturated sample is dried in an oven to vary the saturation. The water saturation is calculated by weighing the sample and comparing the weight with those at full saturations. Then the sample is jacketed and subject to a confining pressure, and gas is injected into the sample up to a given pore pressure. Waveforms are recorded at 80℃ for set 1 and 20℃ for sets 2-3. In the oil-water case, the sample is first fully saturated with oil and then dried in the oven to vary the saturation. Water is injected into the sample up to a given pore pressure.

Waveforms are acquired for sets 1-3 and for aluminum standards (with the same sizes and shapes of the samples) for sets 1 and 3. Waveforms are recorded and velocities are obtained by picking the first arrivals.

Attenuation estimation

We independently applied the spectral-ratio and centroid frequency-shift methods on the same set of compressional waveforms acquired from rocks and reference standards to obtain the quality factors (*Q*). Therefore, the attenuation dependence on the rock/fluid properties can be verified and established through a comparative analysis between the two *Q* sets.

The quality factor *Q* can be determined by the spectral-ratio method (Picotti and Carcione, 2006) using a reference standard material with a very high quality factor (Toksöz *et al.*, 1979; Guo and Fu, 2006) from

$$\ln\left(\frac{A_1(f)}{A_2(f)}\right) = -\frac{\pi x}{QV} f + \ln\frac{G_1(x)}{G_2(x)}, \tag{1}$$

where f is frequency, $A_1(f)$ and $A_2(f)$ are the amplitude spectra of the rock sample and standard material, respectively, Q is the quality factor of the rock sample, x is wave propagation distance, V is the wave velocity and $G_1(x) / G_2(x)$ is the sample/standard geometrical factor.

For set 2, the waveforms were not obtained using the standard material. The attenuation dependence on saturation for each sample is estimated by using the measurement at full gas saturation as a reference,

$$\ln\left(\frac{A_1(f)}{A_2(f)}\right)=-\frac{\pi x}{Q_r V}f+\ln\frac{G_1(x)}{G_2(x)}=\left(\frac{\pi x}{Q_{gas}V_{gas}}-\frac{\pi x}{QV}\right)f+\ln\frac{G_1(x)}{G_2(x)}, \quad (2)$$

where $Q_r=(Q^{-1}-Q_{gas}^{-1}V/V_{gas})^{-1}$ is the relative quality factor, and Q_{gas} and V_{gas} are the quality factor and P-wave velocity at full gas saturation, respectively. A negative Q_r indicates that less attenuation is observed for the considered state than that at full gas saturation.

The centroid frequency-shift method assumes that the amplitude spectrum is subject to a Gaussian distribution (Quan and Harris, 1997; Matsushima *et al.*, 2016), and

$$Q=\frac{\pi\sigma^2\Delta t}{\Delta f_c}, \quad (3)$$

where Δf_c is the difference of centroid frequency between the sample and the reference standard, Δt is the travel-time difference and σ^2 is the spectral variance of the standard.

The compressional waveforms in the siltstone, carbonate, and sandstone samples at different saturations are shown in Figure 1d, 1e and 1f, respectively. It is observed in the siltstone that energy loss increases with increasing gas saturation, and attenuation at full gas-saturation is more significant than that at full liquid saturation, a behavior that differs from the carbonate and sandstone. Four periods of oscillations after the first arrival are used in the spectral-ratio analysis. Figure 1g shows the spectra with the centroid frequencies and Figure 1h shows the spectral-ratio experimental points and least-squares fittings.

Attenuation in siltstones, carbonates and sandstone

For samples L, DS8 and TSM2 at gas-water partial saturation, the measured P-wave attenuation Q^{-1} dependences on saturation (Q^{-1}DS) corresponding to the two methods are given in Figure 2a. The errors of Q^{-1} by the spectral-ratio method are calculated according to Zhubayev *et al.* (2016), which are given in Figure 2a. According to Johnston and Toksöz (1980), the strict interpretation of the errors by fitting a straight line to the spectral ratios only determines the modulation character of the ratios and not the accuracy of the method, which can only be based on reproducibility and comparison with other methods. Both the methods provide similar results, verifying the reliability of the Q estimation. The siltstones generally show a gradual decrease of attenuation with increasing water saturation, which we define as type-A behavior of Q^{-1}DS. On the other hand, in the Q^{-1}DS of the carbonates and sandstone saturated with gas and water, attenuation increases with water saturation and has a peak in the range [51-100] % (we define it as a type-B behavior; e.g. DS8 has a Q^{-1} peak at 79% water saturation in Figure 2a). The Q^{-1}DS and peak-Q^{-1} water saturation of each sample are given in Table 1. In the oil-water tests, no clear trend can be observed for the siltstones (see Table 1).

The relation between the measured P-wave attenuation and porosity at the three full-saturation states are given in Figures 2b (Q^{-1} for the siltstones and sandstone) and 2c (Q_r^{-1} for the carbonates). In most siltstones, higher attenuation can be observed at full gas saturation compared to full oil or full water saturation. Sample D (a silty mudstone) shows significantly less Q^{-1} at full oil saturation than that at full water saturation, a behavior that differs from that of the other siltstones. Figure 2c shows that Q^{-1} at full water saturation is higher than that at full gas saturation (i.e., Q_r^{-1} at full water saturation is positive) for most of the carbonates except for DS2 and DS7, while the relation between Q^{-1} at full oil saturation and that at full water saturation shows no trend. The attenuation dependence on fluid type for each sample is given in Table 1.

Attenuation versus saturation: Experiments and theory

Attenuation dependencies on fluid properties

Most of the published experimental measurements show that attenuation at full liquid saturation (oil, water or brine) is higher than that at full gas saturation or at "dry" (air-saturated) conditions. Moreover, full water saturation shows less attenuation than full oil saturation (e.g., the selected data in Figure 3a). The opposite behavior is shown by Amalokwu *et al.* (2014) for a synthetic sandstone, where attenuation at full gas saturation is higher than that at full water saturation. Aqueous sodium silicate gel was used by Amalokwu *et al.* (2014) to make the silica-cemented synthetic sandstone, which may lead to the intrinsic viscoelasticity of the matrix and cause the high attenuation at full gas saturation. The observed attenuation at full gas saturation in siltstones is higher than that at full liquid saturations (e.g. sample J in Figure 3a).

Figure 3b compares the observed Q^{-1} DSs in K and DS4 with those reported in the literature for different lithologies and frequencies (ultrasonic: Amalokwu *et al.* (2014), 0.65 MHz, Qi *et al.* (2014), 0.5 MHz; seismic: Murphy *et al.* (1982), 571-647 Hz, Yin *et al.* (1992), 700 Hz), while Figure 3c compares those of samples K and DT5 with the trend of typical theoretical models. The published measurements show a type-B behavior with an attenuation peak at high water saturations, which differs with the type-A behavior of the siltstones in the present study. The theoretical or numerical models of patchy-saturation also describe a type-B behavior, and because the fabric heterogeneity is not considered in these models, no attenuation is present at full saturations.

Poroelasticity modeling of attenuation

A double-porosity structure consisting of a host-rock and inclusion frames has been applied by Ba *et al.* (2017) to model the clay squirt-flow mechanism (Marketos and Best, 2010) in siltstones and the crack squirt flow in carbonates. Both the mechanisms are associated with fabric heterogeneity, where the two pore phases (stiff and soft) correspond to the intergranular pores of the host frame and micropores of the clay aggregates, or the intergranular pores and cracks. When compressional wave squeezes a double-porosity rock, fluid flows from soft pores to stiff pores due to the difference of pore compressibility, resulting in wave relaxation.

For a rock partially saturated with gas and water, clay micropores or grain contacts tend to be fully water-saturated due to the water-wettability of minerals and the effect of capillary forces (Li *et al.*, 2001). Therefore, clay and grain contacts/cracks are fully water-saturated, while water is the host fluid and gas is the patch fluid in the intergranular pores. The wave dissipation corresponding to the coupling effects of fabric heterogeneity and patchy saturation can be described with the following equations (Ba *et al.*, 2017):

$$\begin{aligned}&N\nabla^2\mathbf{u}+(A+N)\nabla e+Q_1\nabla(\xi^{(1)}+\phi_2\zeta_{12}+\phi_3\zeta_{13})+Q_2\nabla(\xi^{(2)}-\phi_1\zeta_{12})\\&+Q_3\nabla(\xi^{(3)}-\phi_1\zeta_{13})=\rho_{00}\ddot{\mathbf{u}}+\rho_{01}\ddot{\mathbf{U}}^{(1)}+\rho_{02}\ddot{\mathbf{U}}^{(2)}+\rho_{03}\ddot{\mathbf{U}}^{(3)}\\&+b_1\left(\dot{\mathbf{u}}-\dot{\mathbf{U}}^{(1)}\right)+b_2\left(\dot{\mathbf{u}}-\dot{\mathbf{U}}^{(2)}\right)+b_3\left(\dot{\mathbf{u}}-\dot{\mathbf{U}}^{(3)}\right)\end{aligned}, \tag{4a}$$

$$Q_1\nabla e+R_1\nabla(\xi^{(1)}+\phi_2\zeta_{12}+\phi_3\zeta_{13})=\rho_{01}\ddot{\mathbf{u}}+\rho_{11}\ddot{\mathbf{U}}^{(1)}-b_1\left(\dot{\mathbf{u}}-\dot{\mathbf{U}}^{(1)}\right), \tag{4b}$$

$$Q_2\nabla e+R_2\nabla(\xi^{(2)}-\phi_1\zeta_{12})=\rho_{02}\ddot{\mathbf{u}}+\rho_{22}\ddot{\mathbf{U}}^{(2)}-b_2\left(\dot{\mathbf{u}}-\dot{\mathbf{U}}^{(2)}\right), \tag{4c}$$

$$Q_3\nabla e+R_3\nabla(\xi^{(3)}-\phi_1\zeta_{13})=\rho_{03}\ddot{\mathbf{u}}+\rho_{33}\ddot{\mathbf{U}}^{(3)}-b_3\left(\dot{\mathbf{u}}-\dot{\mathbf{U}}^{(3)}\right), \tag{4d}$$

$$\begin{aligned}&\phi_2(Q_1e+R_1(\xi^{(1)}+\phi_2\zeta_{12}+\phi_3\zeta_{13}))-\phi_1(Q_2e+R_2(\xi^{(2)}-\phi_1\zeta_{12}))\\&=\frac{1}{3}\rho_f^{(1)}\ddot{\zeta}_{12}R_{12}^2\frac{\phi_1^2\phi_2^2\phi_{20}}{\phi_{10}\phi_2}+\frac{1}{3}\dot{\zeta}_{12}R_{12}^2\frac{\eta_f^{(1)}\phi_1^2\phi_2^2\phi_{20}}{\kappa_1\phi_2}\end{aligned}, \tag{4e}$$

$$\begin{aligned}&\phi_3(Q_1e+R_1(\xi^{(1)}+\phi_2\zeta_{12}+\phi_3\zeta_{13}))-\phi_1(Q_3e+R_3(\xi^{(3)}-\phi_1\zeta_{13}))\\&=\frac{1}{3}\rho_f^{(1)}\ddot{\zeta}_{13}R_{13}^2\phi_1^2\phi_3+\frac{1}{3}\dot{\zeta}_{13}R_{13}^2\frac{\eta_f^{(1)}\phi_1^2\phi_3\phi_{10}}{\kappa_1}\end{aligned}, \tag{4f}$$

where $\mathbf{u}$, $\mathbf{U}^{(1)}$, $\mathbf{U}^{(2)}$ and $\mathbf{U}^{(3)}$ are the particle displacements of the rock frame, water in intergranular stiff pores, gas in intergranular stiff pores, and water in soft pores (clay micropores in siltstone, and cracks in carbonate/sandstone), respectively, and e, $\xi^{(1)}$, $\xi^{(2)}$, and $\xi^{(3)}$ are the corresponding displacement divergence fields. The scalar ς_{12} represents the variation of fluid content in squirt flow between stiff pores and soft pores. The scalar ς_{13} represents the variation of fluid content in fluid flow between water-saturated stiff pores and gas-saturated stiff pores. ϕ_{10} is the absolute porosity of the stiff pores. ϕ_{20} is the absolute porosity of the soft pores. ϕ_1, ϕ_2 and ϕ_3 are the relative porosities ($\phi=\phi_1+\phi_2+\phi_3$ is the rock porosity). $\phi_2=v_{\text{clay}}\phi\phi_{20}$ for siltstone (v_{clay} is clay content), and $\phi_2=p(1-\phi)\phi_{20}$ for carbonate/sandstone (p is the volume ratio of cracked grains to all grains). $\phi_3=\phi(1-S_{\text{w}})$ (S_{w} is water saturation). κ_1 is the permeability of the host rock frame. $\eta_f^{(1)}$ and $\rho_f^{(1)}$ are the viscosity and density of the host fluid (water), respectively.

R_{12} is the radius of clay aggregates in siltstones and the radius of compliant cracks in carbonates or sandstone. The gas pocket radius is R_{13}. The stiffnesses A, N, Q_1, Q_2, Q_3, R_1, R_2, R_3, the density coefficients ρ_{00}, ρ_{01}, ρ_{02}, ρ_{03}, ρ_{11}, ρ_{22}, ρ_{33}, and the Biot's dissipation coefficients b_1, b_2, b_3 can be determined in terms of the rock physical properties (Ba *et al.*, 2011, 2017).

By substituting a plane P-wave kernel into equation (4), the Christoffel equation is derived. Its solutions yield the phase velocity and quality factor (Carcione, 2014).

$$V_{\mathrm{P}} = \frac{2\pi f}{\mathrm{Re}(k)}, \quad Q = \frac{\mathrm{Re}(k)}{2\,\mathrm{Im}(k)}. \tag{5}$$

where *f* is the frequency and k is the complex wave number.

Figure 4a shows Q^{-1} as a function of the logarithm of f/κ_1, compared with the experimental data, for the gas-water saturated samples K and DS4. Porosity, permeability and dry-rock density are given in Table 1 and the fluid properties are obtained from Batzle and Wang (1992). For siltstones, the experimental compressional wave velocity V_{P} and Q^{-1} at full gas saturation and full water saturation are used to determine the dry-rock moduli, clay size (R_{12}) and clay bulk modulus. For carbonates and sandstone, the V_{P} and Q^{-1} (Q_{r}^{-1} for set 2) at full water saturation are used. ϕ_{20}=0.02 or 0.09 for the clay or cracks, and v_{clay} is determined from measurements. By adjusting the gas pocket size (R_{13}), the attenuation at partial saturation is modeled. As shown in Figure 4a, the theoretical Q^{-1} agrees well with the experimental data. At ultrasonic frequencies, the full-gas saturated siltstone presents strong dissipation due to the fabric-heterogeneity effect. The two relaxation peaks of fabric heterogeneity and patchy-saturation are separated, with the former dominating in the ultrasonic band, leading to a type-A Q^{-1} DS in siltstones. On the other hand, in the partially-saturated carbonate, the two mechanisms overlap at ultrasonic frequencies, causing a higher attenuation than that at full saturations. The difference in fabric structure between the lithologies results in different behaviors. The mechanism of Biot global flow is incorporated in Equation (4) (Ba *et al.*, 2017), together with the dissipation due to fluid-solid friction along the wave propagation direction, causing the weak Biot peak in the full-gas-saturation curve of DS4 (Fig. 4a). Nitrogen at 10 MPa and 20□ is light in DS4 and the predicted attenuation due to crack squirt flow is negligible.

Figure 4b compares the modeling results with the experiments for the gas-water saturation cases, for type-A (siltstones) and type-B (carbonates and sandstones). The average Q^{-1} DS is given for each type. The modeling results are generally in agreement with the measurements. As shown in Table 1, the measured Q^{-1} DS can be explained by the poroelasticity theory except for samples DS2 and DS8, where more complex structures may exist.

Figure 4c shows theoretical results in agreement with the experimental attenuation dependence on fluid type for all the modeled rocks (the average is given for each lithology), and in general, Q^{-1} at full gas saturation is higher than that at full water saturation for the siltstones, while it is lower than that at full water saturation for the carbonates and sandstone. The model underestimates the carbonate Q^{-1} at full gas saturation (also shown in Figure 4a), suggesting that the crack model is not enough to describe the anelasticity of some carbonates (pore-related clay and bitumen can be observed in the thin section associated with samples DS1-3, DS5-8). Best and Sams (1997) considered the presence of two distinct squirt flow mechanisms (crack- and clay-related) in sandstones and carbonates. We consider only the crack squirt flow in the carbonates and sandstone of this study. The model describes well the observed attenuation in clean dolomites (we assume that the cracks are not completely closed at the tested pressure). However, the theory underestimates Q^{-1} at full gas saturation in set 3 (e.g. see the prediction of DS4 in Figure 4a), which may contain compliant minerals. To incorporate the two squirt-flow mechanisms and patchy-saturation into the same poroelasticity framework will require an extension of the theory.

In this work, the siltstones are measured at a pore pressure of 25 MPa and at 80 ℃, while carbonates and sandstone at 10 MPa and 20 ℃. The difference in fluid properties between the two conditions may affect the attenuation. The red triangles in Figure 4b and 4c give the predictions of the siltstones by substituting the fluid properties at 10 MPa and 20 ℃ in clay squirt-flow modeling. It is shown that with a lighter gas and a more viscous water/oil at 10 MPa and 20 ℃, the ultrasonic P-wave attenuation decreases. However, the general trend of attenuation dependence on saturation or fluid type is consistent with those observed/predicted at 25 MPa and 80 ℃. If the fluids are at a lower pressure (e.g., the ambient conditions), the trend may change, since the gas is too light to cause any attenuation. This case is quite different from that at in-situ (depth) conditions.

In the fully oil-saturated or partially oil-water saturated cases, the observed attenuation dependence on saturation and fluid type are quite complex (Table 1) and our model fails to provide a plausible explanation. Additional effects may be due to the complex geometry of the oil and water patches or the viscoelasticity of oil.

Conclusions

The properties of tight oil reservoirs are different from those of conventional oil and gas reservoirs. In tight oil rocks with strong heterogeneities and small pore channels, the microscopic pore structure and hydrocarbon accumulation are more complex. Wave attenuation is closely related to the rock structure and the presence of pore fluids. Here, we analyze the influence of microstructure and fluid distribution on attenuation. Ultrasonic measurements in rocks saturated with gas and water show that the compressional-wave attenuation decreases with increasing water saturation in tight oil siltstones. The behavior is different for carbonates and sandstone, where attenuation generally increases with water saturation and has a peak at water saturations in the range [51-100] %. For most of the siltstones, the measured attenuation at full gas saturation is higher than that at full liquid saturation, while the behavior is the opposite for most carbonates. The trends for siltstones are also different from those reported in the literature. Poroelasticity theory provides a reasonable explanation of the observed phenomena for gas-water partial saturation. For siltstones, the two loss mechanisms, due to fabric heterogeneity and patchy saturation, have peaks at different frequencies, with the former dominating in the ultrasonic band. On the other hand, for carbonates and sandstones, the relaxation peaks overlap. Modeling with the two different sets of fluid properties matches the general trend of attenuation dependence on saturation/fluid for siltstones at underground conditions. The observed attenuation in partially or fully oil-saturated samples cannot be explained by our model, where other effects may be present, such as pore-fluid viscoelasticity and a complex fluid-patch geometry.

We conclude that the observed attenuation in tight oil siltstones is likely to be the result of squirt-flow, related to its fine-grain characteristics and low permeability. The attenuation in carbonates and sandstones is caused by the mechanisms of patchy-saturation and the two types of squirt flow. The implications obtained here are useful for further studies of attenuation-based geophysical exploration techniques for detecting underground fluids in tight oil reservoir, since the attenuation dependence on saturation is closely associated with lithology, structure and fluid properties.

Wave attenuation plays an important role in applied geophysics for oil and gas exploration. This work shows that the general trend of ultrasonic attenuation dependence on saturation in siltstones is quite different from that observed in carbonates or sandstones. This new trend and phenomena have not been reported in the literature. The interpretation will contribute to a better understanding of attenuation for varying saturation and different lithologies. It is shown that, based on the wave attenuation attribute, dry/gas-saturated tight siltstones can be distinct from liquid-saturated ones. However, it is difficult to identify fluid properties or saturation in tight oil reservoirs partially saturated with oil and water, where the model fails to explain the observed data. This may be related to the low permeability, differences in fluid viscosity and the presence of capillary force. These factors need to be considered to establish a new model for interpreting the observed attenuation in oil-water saturated siltstones.

Experimental measurements explained a poroelasticity model yield the relationship between compressional wave attenuation and pore fluids in tight oil rocks. The characteristic frequency of peak attenuation is shown to be dependent on the heterogeneity scale. Mesoscopic heterogeneities (10^{-4}–10^{-2} m) in actual reservoirs may result in high attenuation in the sonic-seismic frequency band. Although the results obtained from ultrasonic measurements may not be directly applicable at seismic-exploration frequencies, they are instructive for seismic interpretation, because the poroelasticity model can be applied at the seismic frequency band, by considering large-scale heterogeneous inclusions or more viscous liquids.

Acknowledgements

Zhaobing Hao helped in the ultrasonic measurements in rock tests. This work is supported by the Distinguished Professor Program of Jiangsu Province, China, and the Fundamental Research Funds for the Central Universities, China. Experimental waveform data associated with this article can be accessed at https://zenodo.org/record/1240378.

References

Agersborg, R., Johansen, T.A., Jakobsen, M., Sothcott, J., Best, A., 2008. Effects of fluids and dual-pore systems on pressure-dependent velocities and attenuations in carbonates. Geophysics 73, N35-N47.

Adam, L., Batzle, M., Lewallen, K.T., Van Wijk, K., 2009. Seismic wave attenuation in carbonates. J. Geophys. Res., Solid Earth 114, B06208.

Amalokwu, K., Best, I.A., Sothcott, J., Chapman, M., Minshull, T., Li, Y.X., 2014. Water saturation effects on elastic wave attenuation in porous rocks with aligned fractures. Geophys. J. Int. 197, 943-947.

Assefa, S., McCann, C., Sothcott, J., 1999. Attenuation of P- and S-waves in limestones. Geophys. Prospect. 47, 359-392.

Ba, J., Carcione, J.M., Nie, J., 2011. Biot-Rayleigh theory of wave propagation in double-porosity media. J. Geophys. Res., Solid Earth 116, B06202.

Ba, J., Xu, W., Fu, L., Carcione, J.M., Zhang, L., 2017. Rock anelasticity due to patchy saturation and fabric heterogeneity: A double double-porosity model of wave propagation. J. Geophys. Res., Solid Earth 122, 1949-1976.

Ba, J., Zhao, J., Carcione, J.M., Huang, X., 2016. Compressional wave dispersion due to rock matrix stiffening by clay squirt flow. Geophys. Res. Lett. 43, 6186-6195.

Batzle, M.L., Wang, Z., 1992. Seismic properties of pore fluids. Geophysics 57, 1396-1408.

Best, A.I., Sams, M.S., 1997. Compressional wave velocity and attenuation at ultrasonic and sonic frequencies in near-surface sedimentary rocks. Geophys. Prospect. 45, 327-344.

Borgomano, J.V.M., Pimienta, L., Fortin, J., Guéguen, Y., 2017. Dispersion and attenuation measurements of the elastic moduli of a dual-porosity limestone. J. Geophys. Res., Solid Earth 122,2690-2711.

Cadoret, T., Mavko, G., Zinszner, B., 1998. Fluid distribution effect on sonic attenuation in partially saturated limestones. Geophysics, 63,154-160.

Carcione, J.M., 2014. Wave Fields in Real Media. Theory and numerical simulation of wave propagation in anisotropic, anelastic, porous and electromagnetic media, 3rd ed., Elsevier Sci., Amsterdam.

Cao, Z., Liu, G., Zhan, H., Gao, J., Zhang, J., Li, C., Xiang, B., 2017. Geological roles of the siltstones in tight oil play of Permian Lucaogou Formation in Jimusar Sag, Junggar Basin. Mar. Petrol. Geol. 83, 333-344.

Chapman, S., Tisato, N., Quintal, B., Holliger, K., 2016. Seismic attenuation in partially saturated Berea sandstone submitted to a range of confining pressures. J. Geophys. Res., Solid Earth 121, 1664-1676.

Clarkson, C.R., Jensen, J.L., Pedersen, P.K., Freeman, M., 2012. Innovative methods for flow-unit and pore-structure analyses in a tight siltstone and shale gas reservoir. AAPG Bulletin, 96, 355-374.

Dvorkin, J., Nur, A., 1996. Elasticity of high-porosity sandstones: Theory for two North Sea data sets. Geophysics 61,1363-1370.

Glubokovskikh, S., Gurevich, B., 2017. Effect of grain-scale gas patches on the seismic properties of double porosity rocks. Geophys. J. Int. 208, 432-436.

Guo, M., Fu, L., 2006. Stress associated coda attenuation from ultrasonic waveform measurements. Geophys. Res. Lett. 34, L09307.

Guo, M., Fu, L., Ba, J., 2009. Comparison of stress-associated coda attenuation and intrinsic attenuation from ultrasonic measurements. Geophys. J. Int. 178: 447-456.

Helle, H.B., Pham, N.H., Carcione, J.M., 2003. Velocity and attenuation in partially saturated rocks: poroelastic numerical experiments. Geophys. Prospect. 51, 551-566.

Jia, C., Zheng, M., Zhang, Y., 2012. Unconventional hydrocarbon resources in China and the prospect of exploration and development. Petrol. Explor. Dev. 39(2), 139–146.

Johnston, D.H., Toksöz, M.N., 1980. Ultrasonic P and S wave attenuation in dry and saturated rocks under pressure. J. Geophys. Res., Solid Earth 85, 925-936.

King, M.S., 2005. Rock-physics developments in seismic exploration: A personal 50-year perspective. Geophysics 70, 3ND-8ND.

Kuteynikova, M., Tisato, N., Jänicke, R., Quintal, B., 2014. Numerical modeling and laboratory measurements of seismic attenuation in partially saturated rock. Geophysics 79, L13-L20.

Li, X., Zhong, L., Pyrak-Nolte, L.J., 2001. Physics of partially saturated porous media: Residual saturation and seismic-wave propagation. Annu. Rev. Earth Planet. Sci. 29, 419-460.

Marketos, G., Best, A.I., 2010. Application of the BISQ model to clay squirt flowin reservoir sandstones. J. Geophys. Res., Solid Earth 115, B06209.

Matsushima, J., Suzuki, M., Kato, Y., Rokugawa, S., 2016. Ultrasonic measurements of attenuation and velocity of compressional and shear waves in partially frozen unconsolidated sediment and synthetic porous rock. Geophysics 81, D141–D153.

Murphy, W.F. 1982. Effects of partial water saturation on attenuation in Massilon sandstone and Vycor porous glass. J. Acoust. Soc. Am. 71, 639-648.

Müller, T.M., Gurevich, B., 2004. One-dimensional random patchy saturation model for velocity and attenuation in porous rocks. Geophysics 69, 1166-1172.

Müller, T.M., Toms-Stewart, J., Wenzlau, F., 2008. Velocity-saturation relation for partially saturated rocks with fractal pore fluid distribution. Geophys. Res. Lett. 26, L09306.

Norris, A.N., 1993. Low-frequency dispersion and attenuation in partially saturated rocks. J. Acoust. Soc. Am. 94, 359-370.

Nur, A., Wang, Z., 2001. Seismic and acoustic velocities in reservoir rocks: Volume 1: Experimental studies. Society of Exploration Geophysics, Tulsa.

Picotti, S., Carcione, J.M., 2006. Estimating seismic attenuation (Q) in the presence of random noise. J. Seism. Explor. 15, 165-181.

Qi, Q., Müller, T. M., Gurevich, B., Lopes, S., Lebedev, M., Casapari, E., 2014. Quantifying the effect of capillarity on attenuation and dispersion in patchy-saturated rocks. Geophysics 79, WB35-WB50.

Quan, Y., Harris, J.M., 1997. Seismic attenuation tomography using the frequency shift method. Geophysics 62, 895-905.

Sun, W., Ba, J., Müller, T.M., Carcione, J.M., Cao, H., 2014. Comparison of P-wave attenuation models of wave-induced flow. Geophys. Prospect. 63, 378-390.

Tao, G., King, M.S., Nabi-Bidhendi, M., 1995. Ultrasonic wave propagation in dry and brine-saturated sandstones as a function of effective stress: laboratory measurements and modelling. Geophys. Prospect. 43, 299-327.

Toksöz, M.N, Johnston, D.H., Timur, A., 1979. Attenuation of seismic waves in dry and saturated rocks: I. Laboratory measurements. Geophysics 44, 681-690.

White, J.E., 1975. Computed seismic speeds and attenuation in rocks with partial gas saturation. Geophysics 40, 224-232.

Winkler, K., Nur, A., 1979. Pore fluids and seismic attenuation in rocks. Geophys. Res. Lett. 6, 1-4.

Winkler, K.W., Nur, A., 1982. Seismic attenuation: Effects of pore fluids and frictional-sliding. Geophysics 47, 1-15.

Wu, H., Zhang, C., Ji, Y., Liu, R., Wu, H., Zhang, Y., Geng, Z., Zhang, Y., Yang, J., 2018. An improved method of characterizing the pore structure in tight oil reservoirs: integrated NMR and constant-rate-controlled porosimetry data. J. Pet. Sci. Eng. 166, 778-796.

Yin, C.S., Batzle, M.L., Smith, B.J., 1992. Effects of partial liquid/gas saturation on extensional wave attenuation in Berea sandstone. Geophys. Res. Lett. 19, 1399-1402.

Zhubayev, A., Houben, M.E., Smeulders, D.M.J., Barnhoorn, A., 2016. Ultrasonic velocity and attenuation anisotropy of shales, Whitby, United Kingdom. Geophysics 81, D45-D56.

Zou, C., Zhang, G., Yang, Z., Tao, S., Hou, L., Zhu, R., Yuan, X., Ran, Q., Li, D., Wang, Z., 2013. Concepts, characteristics, potential and technology of unconventional hydrocarbons: On unconventional petroleum geology. Petrol. Explor. Dev. 40(4), 413-428.

Figure Captions:

Figure 1. (a) SEM analyses on the siltstone from the target formation show pore-related clay forming a secondary micro-porous medium; Thin section analyses on the dolomite (b) and the tight sandstone (c) show grain contacts or microcracks connected to intergranular pores; Measured ultrasonic compressional waveforms in sample K and the corresponding standard (d), sample DS4 (e), and sample TSM2 (f) with different fluids and saturations (for each waveform, the first arrival and the end of the first four periods are indicated, and the time window between them is used in the attenuation analysis); (g) Amplitude spectra of P-waves in K at different saturation states (centroid frequencies are labeled); (h) Best least-square fits of the logarithm of the spectral ratios in K.

Figure 2. (a) P-wave attenuation dependence on saturation estimated with the spectral-ratio (SR) and centroid frequency-shift (CFS) methods in the gas-water partially-saturated L, DS8 and TSM2 (measurements are performed at six intermediate saturations for sample set 1, and seven intermediate saturations for sets 2 and 3; error bars are given for the SR estimation results); (b) Measured Q^{-1} as a function of porosity for the clastic rocks at the full gas, water and oil saturation states; (c) Measured Q_{r}^{-1} as a function of porosity for the carbonates. $Q^{-1}/Q_{\mathrm{r}}^{-1}$ in Figure 2b/2c is estimated by using the SR method and then verified with CFS method.

Figure 3. (a) Measured P-wave attenuation dependence on fluid type in samples J and DS4 compared to published experimental results; (b) Measured attenuation dependence on saturation in gas-water partially-saturated K and DS4, compared to published experimental results; (c) Measured attenuation (Q_{r}^{-1}) dependence on saturation in gas-water partially-saturated K and DT5, compared with the trend of typical curves of theoretical models published in the scientific

literature. Porosity is given for each sample/model.

Figure 4. (a) Modeling results of attenuation as a function of the logarithm of frequency divided by permeability in K and DS4, compared to the experimental data (each peak is labelled with the corresponding mechanism); (b) Averaged attenuation dependences on saturation predicted by the theory and the experimental data of type-A, compared to those of type-B (red triangles give another set of type-A predictions of the siltstones by substituting the fluid properties at 10 MPa and 20℃); (c) Averaged attenuation dependence on fluid type for different rock types predicted by the theory and compared to the experimental data (red triangles give another set of predictions of the siltstones by substituting the fluid properties at 10 MPa and 20℃).

Table Caption:

Table 1. Rock properties and Q^{-1} measurements (Q^{-1}s are estimated by the spectral-ratio method and then verified with the centroid frequency-shift method), compared with the theoretical results. Type-A of Q^{-1} dependence of saturation (Q^{-1}DS): a gradual decrease of attenuation with increasing water saturation; Type-B of Q^{-1}DS: increasing attenuation with water saturation, peaking at high water saturation. Q^{-1}_{gas}: Q^{-1} at full gas saturation; Q^{-1}_{water}: Q^{-1} at full water saturation; Q^{-1}_{oil}: Q^{-1} at full oil saturation.

Table 1.

Sample	Lithology	Porosity (%)	Permeability (md)	Dry density (g/cm^3)	Q^{-1}DS (Water-gas partial-saturation experiment)	Q^{-1}DS (Water-gas partial-saturation modeling)	Peak-Q^{-1} water saturation in water-gas partial-saturation measurements	Q^{-1}DS (Water-oil partial-saturation experiment)	Q^{-1} dependence of fluid type (Full-saturation experiment)	Q^{-1} dependence of fluid type (Full-saturation modeling)
A; set 1	Muddy Siltstone	2.88	0.0045	2.61	-	-	-	-	$Q_{water}^{-1}\&Q_{oil}^{-1}>Q_{gas}^{-1}$	$Q_{water}^{-1}\&Q_{oil}^{-1}>Q_{gas}^{-1}$
B; set 1	Muddy Siltstone	4.6	0.38	2.56	-	-	-	-	$Q_{gas}^{-1}>Q_{water}^{-1}\&Q_{oil}^{-1}$	$Q_{water}^{-1}\&Q_{oil}^{-1}>Q_{gas}^{-1}$
C; set 1	Siltstone	5.2	0.019	2.58	-	-	-	-	$Q_{gas}^{-1}>Q_{water}^{-1}\&Q_{oil}^{-1}$	$Q_{gas}^{-1}>Q_{water}^{-1}\&Q_{oil}^{-1}$
D; set 1	Silty Mudstone	5.56	0.011	2.53	-	-	-	-	$Q_{water}^{-1}>Q_{gas}^{-1}>Q_{oil}^{-1}$	$Q_{water}^{-1}>Q_{gas}^{-1}>Q_{oil}^{-1}$
E; set 1	Siltstone	5.6	0.017	2.52	-	-	-	-	$Q_{gas}^{-1}>Q_{water}^{-1}\&Q_{oil}^{-1}$	$Q_{gas}^{-1}>Q_{water}^{-1}\&Q_{oil}^{-1}$
F; set 1	Siltstone	5.79	0.035	2.41	-	-	-	-	$Q_{gas}^{-1}>Q_{water}^{-1}\&Q_{oil}^{-1}$	$Q_{gas}^{-1}>Q_{water}^{-1}\&Q_{oil}^{-1}$
G; set 1	Siltstone	5.8	0.02	2.55	-	-	-	-	$Q_{gas}^{-1}>Q_{water}^{-1}\&Q_{oil}^{-1}$	$Q_{gas}^{-1}>Q_{water}^{-1}\&Q_{oil}^{-1}$
H; set 1	Siltstone	6.45	0.097	2.38	A	A	0	No trend	$Q_{gas}^{-1}>Q_{water}^{-1}\&Q_{oil}^{-1}$	$Q_{gas}^{-1}>Q_{water}^{-1}\&Q_{oil}^{-1}$
I; set 1	Siltstone	10.87	0.39	2.29	A	A	0	No trend	$Q_{gas}^{-1}>Q_{water}^{-1}\&Q_{oil}^{-1}$	$Q_{gas}^{-1}>Q_{water}^{-1}\&Q_{oil}^{-1}$
J; set 1	Muddy Siltstone	12.75	0.17	2.3	A	A	0.13	No trend	$Q_{gas}^{-1}>Q_{water}^{-1}\&Q_{oil}^{-1}$	$Q_{gas}^{-1}>Q_{water}^{-1}\&Q_{oil}^{-1}$
K; set 1	Siltstone	13.09	0.08	2.28	A	A	0	No trend	$Q_{gas}^{-1}>Q_{water}^{-1}\&Q_{oil}^{-1}$	$Q_{gas}^{-1}>Q_{water}^{-1}\&Q_{oil}^{-1}$
L; set 1	Siltstone	13.97	0.084	2.26	A	A	0	No trend	$Q_{gas}^{-1}>Q_{water}^{-1}\&Q_{oil}^{-1}$	$Q_{gas}^{-1}>Q_{water}^{-1}\&Q_{oil}^{-1}$
DT1; set 2	Clean dolomite	5.10	0.091	2.69	B	B	1	A	$Q_{water}^{-1}\&Q_{oil}^{-1}>Q_{gas}^{-1}$	$Q_{water}^{-1}\&Q_{oil}^{-1}>Q_{gas}^{-1}$
DT2; set 2	Clean dolomite	5.34	0.458	2.66	B	B	0.85	A	$Q_{water}^{-1}\&Q_{oil}^{-1}>Q_{gas}^{-1}$	$Q_{water}^{-1}\&Q_{oil}^{-1}>Q_{gas}^{-1}$
DT3; set 2	Clean dolomite	5.47	0.174	2.67	B	B	0.89	A	$Q_{water}^{-1}\&Q_{oil}^{-1}>Q_{gas}^{-1}$	$Q_{water}^{-1}\&Q_{oil}^{-1}>Q_{gas}^{-1}$
DT4; set 2	Clean dolomite	12.08	162.753	2.41	B	B	0.86	A	$Q_{water}^{-1}\&Q_{oil}^{-1}>Q_{gas}^{-1}$	$Q_{water}^{-1}\&Q_{oil}^{-1}>Q_{gas}^{-1}$
DT5; set 2	Clean dolomite	12.28	22.819	2.44	B	B	0.88	A	$Q_{water}^{-1}\&Q_{oil}^{-1}>Q_{gas}^{-1}$	$Q_{water}^{-1}\&Q_{oil}^{-1}>Q_{gas}^{-1}$
DS1; set 2	Dolomite	11.63	0.661	2.45	B	B	0.61	A	$Q_{water}^{-1}\&Q_{oil}^{-1}>Q_{gas}^{-1}$	$Q_{water}^{-1}\&Q_{oil}^{-1}>Q_{gas}^{-1}$
DS2; set 2	Dolomite	11.73	0.138	2.51	No trend	-	0	A	$Q_{gas}^{-1}>Q_{water}^{-1}\&Q_{oil}^{-1}$	-
DS3; set 2	Dolomite	11.75	0.075	2.45	B	B	0.89	A	$Q_{water}^{-1}\&Q_{oil}^{-1}>Q_{gas}^{-1}$	$Q_{water}^{-1}\&Q_{oil}^{-1}>Q_{gas}^{-1}$
DS4; set 3	Dolomite	16.87	3.31	2.32	B	B	0.51	No trend	$Q_{water}^{-1}\&Q_{oil}^{-1}>Q_{gas}^{-1}$	$Q_{water}^{-1}\&Q_{oil}^{-1}>Q_{gas}^{-1}$
DS5; set 3	Dolomite	4.99	1.34	2.67	B	B	0.67	No trend	$Q_{water}^{-1}\&Q_{oil}^{-1}>Q_{gas}^{-1}$	$Q_{water}^{-1}\&Q_{oil}^{-1}>Q_{gas}^{-1}$
DS6; set 3	Dolomite	6.93	0.601	2.64	B	B	0.77	B	$Q_{water}^{-1}>Q_{gas}^{-1}>Q_{oil}^{-1}$	$Q_{water}^{-1}\&Q_{oil}^{-1}>Q_{gas}^{-1}$
DS7; set 3	Dolomite	10.37	1.430	2.52	A	-	0	B	$Q_{gas}^{-1}>Q_{water}^{-1}\&Q_{oil}^{-1}$	-
DS8; set 3	Dolomite	6.08	0.130	2.65	B	B	0.79	B	$Q_{water}^{-1}>Q_{gas}^{-1}>Q_{oil}^{-1}$	$Q_{water}^{-1}\&Q_{oil}^{-1}>Q_{gas}^{-1}$
TSM2; set 3	Tight sandstone	8.64	0.38	2.41	B	B	0.89	-	$Q_{water}^{-1}\&Q_{oil}^{-1}>Q_{gas}^{-1}$	$Q_{water}^{-1}\&Q_{oil}^{-1}>Q_{gas}^{-1}$

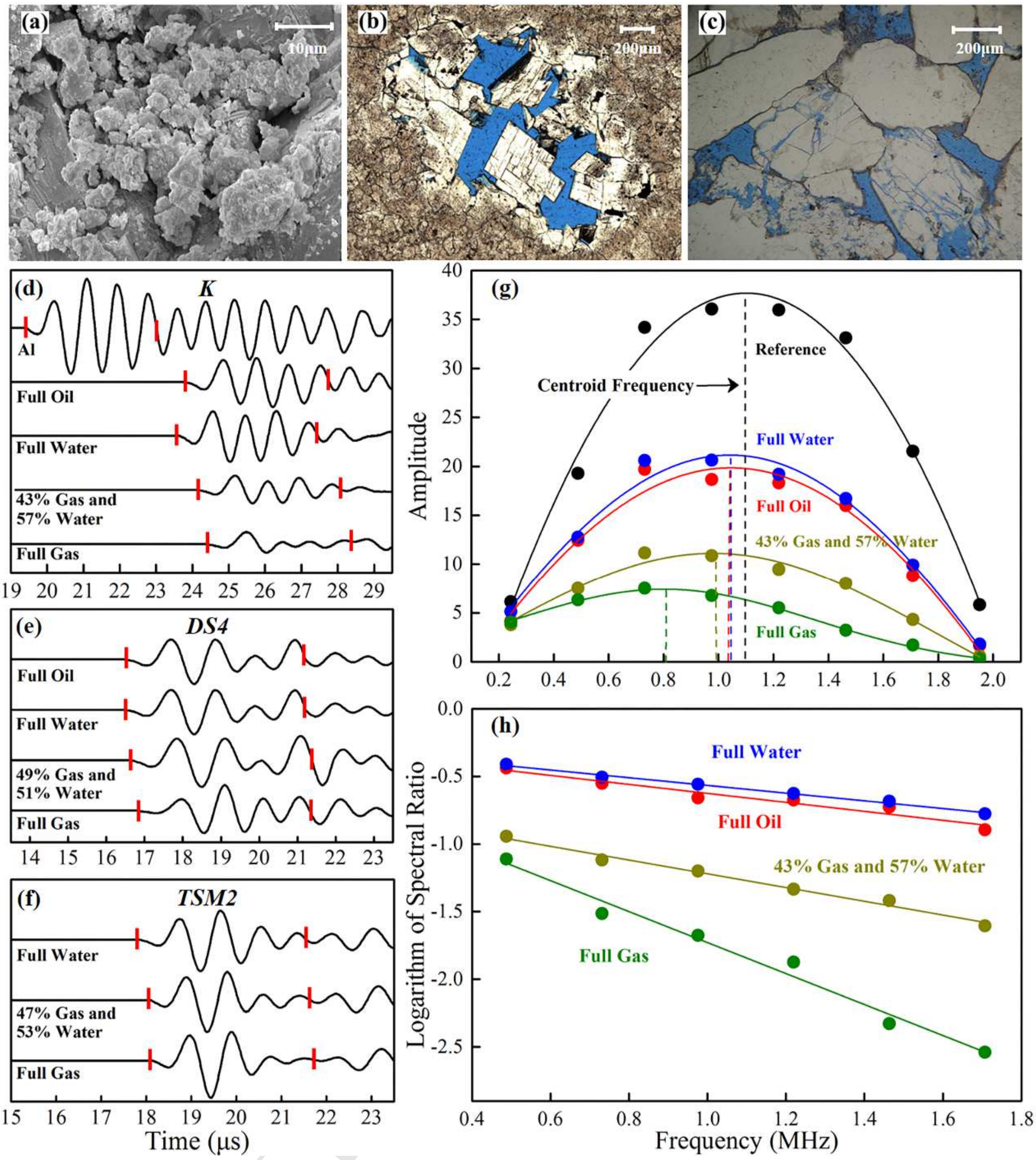
(a)
10μm
(b)
200μm
(c)
200μm
(d)
K
Al
Full Oil
Full Water
43% Gas and
57% Water
Full Gas
(e)
DS4
Full Oil
Full Water
49% Gas and
51% Water
Full Gas
(f)
TSM2
Full Water
47% Gas and
53% Water
Full Gas
Time (μs)
(g)
Reference
Centroid Frequency
Full Water
Full Oil
43% Gas and 57% Water
Full Gas
Amplitude
(h)
Full Water
Full Oil
43% Gas and 57% Water
Full Gas
Logarithm of Spectral Ratio
Frequency (MHz)

Figure 1.

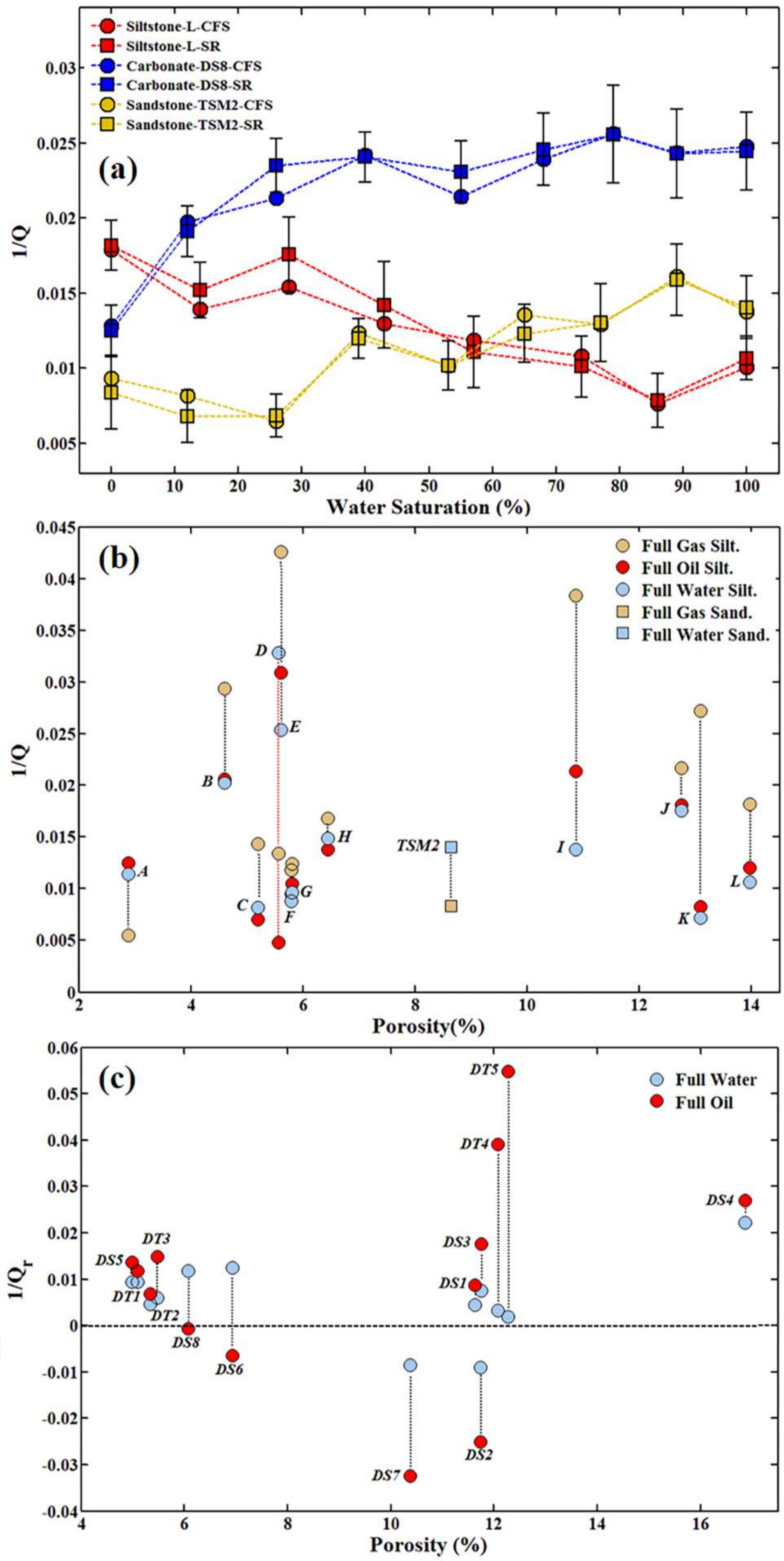

534

535 **Figure 2**.

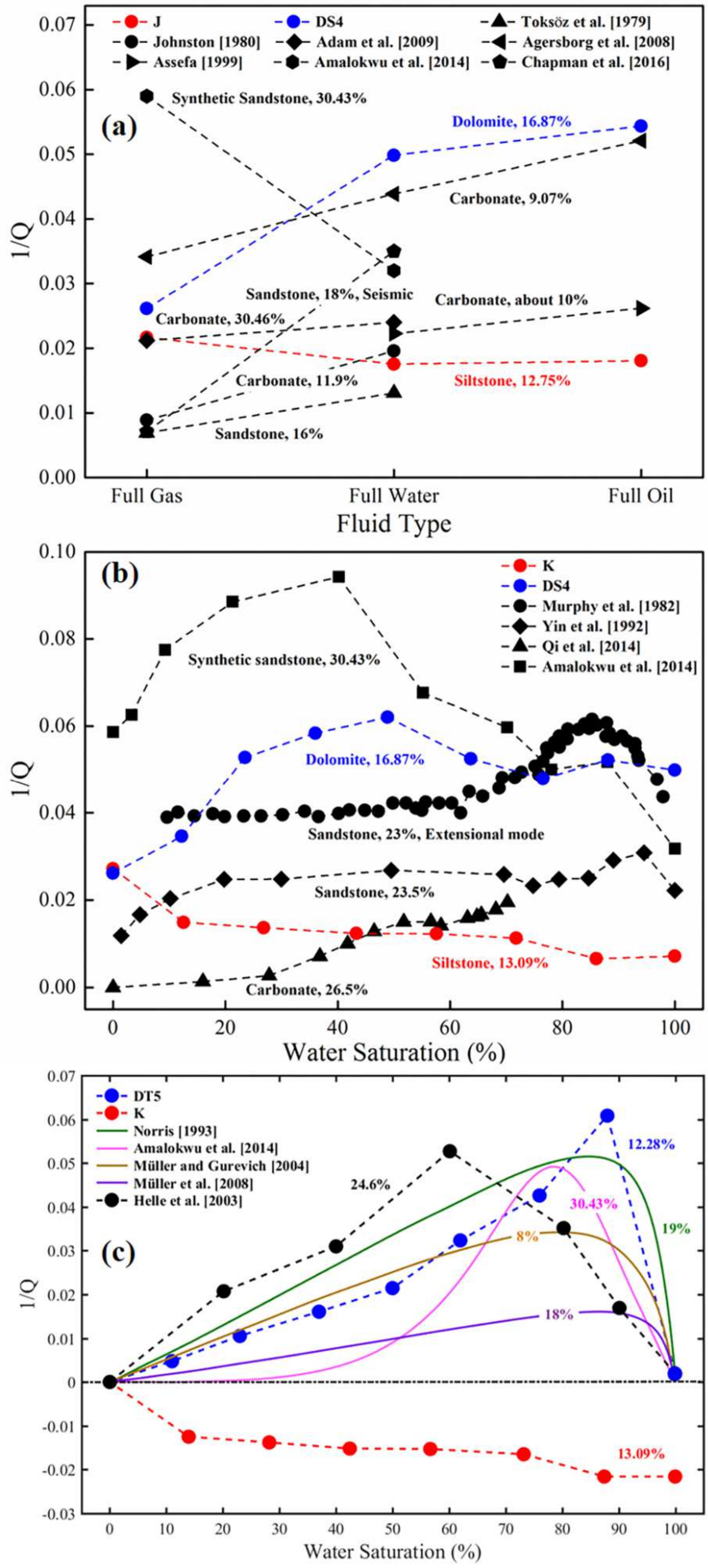

536

537 **Figure 3**.

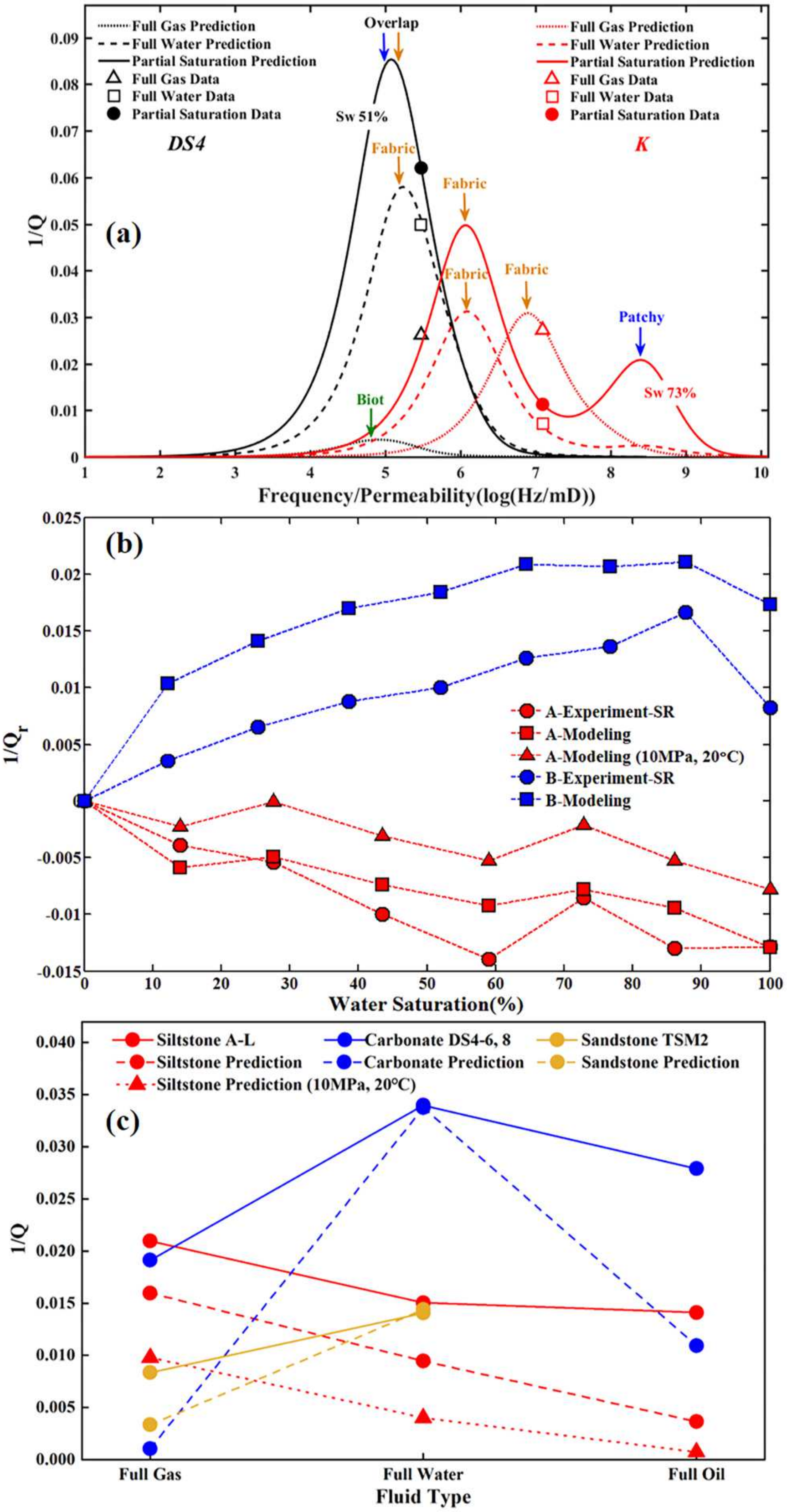

Full Gas Prediction
Full Water Prediction
Partial Saturation Prediction
Full Gas Data
Full Water Data
Partial Saturation Data
DS4
K
Overlap
Sw 51%
Fabric
Patchy
Sw 73%
Biot
(a)
1/Q
Frequency/Permeability(log(Hz/mD))
(b)
$1/Q_r$
A-Experiment-SR
A-Modeling
A-Modeling (10MPa, 20°C)
B-Experiment-SR
B-Modeling
Water Saturation(%)
(c)
Siltstone A-L
Siltstone Prediction
Siltstone Prediction (10MPa, 20°C)
Carbonate DS4-6, 8
Carbonate Prediction
Sandstone TSM2
Sandstone Prediction
1/Q
Full Gas
Full Water
Full Oil
Fluid Type

Figure 4.

Highlights

1. Ultrasonic P-wave attenuation decreases with water saturation in in-situ water-gas partially-saturated siltstones.
2. Attenuation behavior with fluid type and saturation in tight oil siltstones differ from those of carbonates and sandstones.
3. Poroelasticity modeling by incorporating fabric and fluid heterogeneities explains the observed phenomena in water-gas saturated siltstones.